Ultrabroadband radio-frequency arbitrary waveform generation with high-speed phase and amplitude modulation capability

Amir Rashidinejad,* Daniel E. Leaird, and Andrew M. Weiner

School of Electrical and Computer Engineering, Purdue University, 465 Northwestern Avenue, West Lafayette, Indiana 47907-2035, USA

arashidi@purdue.edu

Abstract: We introduce a novel photonic-assisted ultrabroadband radio-frequency arbitrary waveform generation setup capable of high-speed phase and amplitude modulation of the individual arbitrary waveforms. The waveform generator is based on an optical interferometer, within which a high-resolution optical pulse shaper and integrated optic phase and intensity modulators are placed, followed by frequency-to-time mapping. The phase and amplitude of each ultrabroadband waveform within the generated sequence can be continuously tuned by adjusting the driving voltages applied to the phase and intensity modulator pair, hence overcoming the slow update speed of conventional spatial light modulator-based pulse shapers. Moreover, this data modulation is completely independent from and does not interfere with RF waveform design. Programmable ultrabroadband RF sequences, spanning more than 4.7 octaves from 2 to 52 GHz, are modulated with real-time data in up to 16 level, M-ary phase-shift keying and quadrature amplitude modulation formats.

OCIS codes: (060.5625) Radio frequency photonics; (320.5540) Pulse shaping; (060.4080) Modulation; (060.5060) Phase modulation.

References and links

1. J. Capmany and D. Novak, "Microwave photonics combines two worlds," Nat. Photonics **1**(6), 319–330 (2007).
2. J. P. Yao, "Microwave photonics," J. Lightwave Technol. **27**(3), 314–335 (2009).
3. M. Li, J. Azaña, N. Zhu, and J.-P. Yao, "Recent progresses on optical arbitrary waveform generation," Frontiers of Optoelectronics **7**(3), 359–375 (2014).
4. S. Hardy, "Keysight technologies offers 65-GSa/s, 20-GHz arbitrary waveform generator," Lightwave Online. **31**(5), (2014).
5. T. Yilmaz, C. M. DePriest, T. Turpin, J. H. Abeles, and P. J. Delfyett, "Toward a photonic arbitrary waveform generator using modelocked external cavity semiconductor laser," IEEE Photon. Technol. Lett. **14**(11), 1608–1610 (2002).
6. J. Chou, Y. Han, and B. Jalali, "Adaptive RF-photonic arbitrary waveform generator," IEEE Photon. Technol. Lett. **15**(4), 581–583 (2003).
7. I. S. Lin, J. D. McKinney, and A. M. Weiner, "Photonic synthesis of broadband microwave arbitrary waveforms applicable to ultra-wideband communication," IEEE Microw. Wirel. Compon. Lett. **15**(4), 226–228 (2005).
8. A. Zeitouny, S. Stepanov, O. Levinson, and M. Horowitz, "Optical generation of linearly chirped microwave pulses using fiber Bragg gratings," IEEE Photon. Technol. Lett. **17**(3), 660–662 (2005).
9. J. Azana, N. K. Berger, B. Levit, and B. Fischer, "Broadband arbitrary waveform generation based on microwave frequency upshifting in optical fibers," J. Lightwave Technol. **24**(7), 2663–2675 (2006).
10. Y. Dai, X. Chen, H. Ji, and S. Xie, "Optical arbitrary waveform generation based on sampled fiber Bragg gratings," IEEE Photon. Technol. Lett. **19**(23), 1916–1918 (2007).
11. C. Wang and J. P. Yao, "Photonic generation of chirped millimeter-wave pulses based on nonlinear frequency-to-time mapping in a nonlinearly chirped fiber bragg grating," IEEE Trans. Microw. Theory Tech. **56**(2), 542–553 (2008).
12. V. Torres-Company, J. Lancis, P. Andrés, and L. R. Chen, "20 GHz arbitrary radio-frequency waveform generator based on incoherent pulse shaping," Opt. Express **16**(26), 21564–21569 (2008).
13. C. B. Huang, D. E. Leaird, and A. M. Weiner, "Synthesis of millimeter-wave power spectra using time-multiplexed optical pulse shaping," IEEE Photon. Technol. Lett. **21**(18), 1287–1289 (2009).

#235746 - $15.00 USD Received 5 Mar 2015; revised 20 Apr 2015; accepted 25 Apr 2015; published 30 Apr 2015

14. R. Ashrafi, Y. Park, and J. Azana, "Fiber-based photonic generation of high-frequency microwave pulses with reconfigurable linear chirp control," IEEE Trans. Microw. Theory Tech. **58**(11), 3312–3319 (2010).
15. C. Wang and J. P. Yao, "Large time-bandwidth product microwave arbitrary waveform generation using a spatially discrete chirped fiber Bragg grating," J. Lightwave Technol. **28**(11), 1652–1660 (2010).
16. M. Li and J. P. Yao, "Photonic generation of continuously tunable chirped microwave waveforms based on a temporal interferometer incorporating an optically-pumped linearly-chirped fiber bragg grating," IEEE Trans. Microw. Theory Tech. **59**(12), 3531–3537 (2011).
17. J. W. Shi, F. M. Kuo, C. Nan-Wei, S. Y. Set, C. B. Huang, and J. E. Bowers, "Photonic generation and wireless transmission of linearly/nonlinearly continuously tunable chirped millimeter-wave waveforms with high time-bandwidth product at W-Band," IEEE Photon. J. **4**(1), 215–223 (2012).
18. A. Dezfooliyan and A. M. Weiner, "Photonic synthesis of high fidelity microwave arbitrary waveforms using near field frequency to time mapping," Opt. Express **21**(19), 22974–22987 (2013).
19. A. Rashidinejad and A. M. Weiner, "Photonic radio-frequency arbitrary waveform generation with maximal time-bandwidth product capability," J. Lightwave Technol. **32**(20), 3383–3393 (2014).
20. T. Kleine-Ostmann and T. Nagatsuma, "A review on terahertz communications research," J. Infrared, Millim. Terahertz Waves **32**(2), 143–171 (2011).
21. T. Nagatsuma, S. Horiguchi, Y. Minamikata, Y. Yoshimizu, S. Hisatake, S. Kuwano, N. Yoshimoto, J. Terada, and H. Takahashi, "Terahertz wireless communications based on photonics technologies," Opt. Express **21**(20), 23736–23747 (2013).
22. A. J. Seeds, M. J. Fice, K. Balakier, M. Natrella, O. Mitrofanov, M. Lamponi, M. Chtioui, F. van Dijk, M. Pepper, G. Aeppli, A. G. Davies, P. Dean, E. Linfield, and C. C. Renaud, "Coherent terahertz photonics," Opt. Express **21**(19), 22988–23000 (2013).
23. A. J. Seeds, "TeraHertz photonics for communications," in *Optical Fiber Communication Conference*, OSA Technical Digest (online), Invited Talk Th4H.1, (2014).
24. A. M. Weiner, A. Dezfooliyan, Y. Li, and A. Rashidinejad, "Selected advances in photonic ultrabroadband radio-frequency arbitrary waveform generation," *International Topical Meeting on Microwave Photonics* (*MWP*), 325–328, (2013).
25. Y. Li, A. Dezfooliyan, and A. M. Weiner, "Photonic synthesis of spread spectrum radio frequency waveforms with arbitrarily long time apertures," J. Lightwave Technol. **32**(20), 3580–3587 (2014).
26. Y. Li, A. Rashidinejad, J.-M. Wun, D. E. Leaird, J.-W. Shi, and A. M. Weiner, "Photonic generation of W-band arbitrary waveforms with high time-bandwidth products enabling 3.9mm Range Resolution," Optica **1**(6), 446–454 (2014).
27. V. Torres-Company, D. E. Leaird, and A. M. Weiner, "Dispersion requirements in coherent frequency-to-time mapping," Opt. Express **19**(24), 24718–24729 (2011).
28. M. D. McKinley, K. A. Remley, M. Myslinski, J. S. Kenney, D. Schreurs, and B. Nauwelaers, "EVM calculations for broadband modulated signals," in *Proceedings of 64th ARFTG Conference*, (Orlando, 2004), 45–52.
29. A. Kaneko, H. Yamazaki, and Y. Miyamoto, "Linear optical modulator," in *Optical Fiber Communication Conference*, OSA Technical Digest (online), Invited Talk W3K.5, (2014).
30. J. Proakis and M. Salehi, *Digital Communications* (McGraw-Hill, 2007).

1. Introduction

Generation of programmable microwave and millimeter-wave (MMW) waveforms with bandwidths over tens of gigahertz has many potential applications, from ultrahigh-speed wireless communication to high resolution ranging and electromagnetic imaging [1–3]. Due to digital-to-analog convertor speed limitations, state-of-the art electronic RF-arbitrary waveform generators (RF-AWG) are currently incapable of high-frequency and wideband waveform generation beyond 20 GHz [4]. Photonic-assisted RF generation schemes, however, do not suffer from such restrictions and outperform electronics in terms of scaling to such high frequencies [5–21].

Among the many photonic-assisted RF generation techniques, photonic RF-AWG based on optical pulse shaping and frequency-to-time mapping (FTM) have been the most developed [6,7,12,18,19]. The main underlying component in all these schemes is an optical pulse shaper, usually based on liquid crystal spatial light modulators (SLMs), that shapes the spectral content of a short optical pulse. Although current pulse shapers are programmable in amplitude and phase, their update speed is relatively slow, making them incompatible with most practical data modulation rates. Thus, SLM-based RF-AWG techniques require some other means of restructuring in order to implement high-speed data modulation.

RF-photonic techniques have also been extensively utilized to enable high-speed and high-complexity data modulation for wireless communications, especially in the MMW and

#235746 - $15.00 USD Received 5 Mar 2015; revised 20 Apr 2015; accepted 25 Apr 2015; published 30 Apr 2015

sub-terahertz frequency regimes [20–23]. These systems typically modulate two or more appropriately-spaced optical carriers in order to implement complex data modulation on a single or several RF carriers at high frequency bands. However, the combination of high-speed data modulation and RF-arbitrary waveform generation has seen little attention. Enabling high-speed data modulation on the generated RF-AWG waveforms not only allows the possibility of high-speed data communications over ultrabroadband channels, but also offers potential for utilizing these programmable waveforms in applications such as long-range unambiguous radar and covert wireless communications with high coding gains in highly dispersive and multipath environments. As an example, our group has previously reported a technique that utilizes two optical pulse shapers and allows high-speed binary data modulation of photonic-assisted RF-AWG, with experimental demonstrations of their applications in highly-dispersive ultrabroadband RF channel sounding and high resolution RF ranging with extended non-ambiguous range [24–26].

In this paper, we introduce a novel photonic RF-AWG setup capable of applying high-speed phase and amplitude modulation on the individual ultrabroadband RF arbitrary waveforms. The proposed setup is an extension of a recently-reported RF-AWG system based on an optical interferometer architecture, that is capable of generating programmable RF waveforms with high time-bandwidth product and widely tunable center frequency [19,26]. This data modulation scheme is completely independent of the RF-AWG stage, allowing immediate incorporation of real-time data modulation on the generated RF waveforms. Experimentally, we report direct measurements of phase- and amplitude-modulated ultrabroadband waveform sequences with frequency content from ~2 GHz to ~52 GHz, spanning more than 4.7 octaves.

2. Radio-frequency arbitrary waveform generation principle

The schematic for our photonic-assisted RF-AWG configuration is depicted in Fig. 1. The system consists of an ultrafast pulsed laser source, an optical interferometric subsystem, a quadratic dispersive element, and a high-speed photodetector (PD). In this design the optical interferometer has a dual utility. The bottom arm of the interferometer includes a high-resolution optical pulse shaper and a variable optical delay line (VDL) to provide RF-arbitrary waveform generation. The center frequency and the temporal profile of the generated RF waveforms are controlled by tuning the VDL and by modifying the pulse shaper transfer function, respectively, as explained in [19]. The top arm includes high-speed optical phase and intensity modulators (PM and IM), which are used to achieve programmable phase and amplitude modulation on individual RF waveforms within the generated sequence. Although similar results can be achieved using an optical in-phase/quadrature (I/Q) modulator, here we simply consider an IM and PM already available in our laboratory in series. Two independent electrical pattern streams, synchronized with the repetition rate of the optical source, are utilized to apply multilevel sequences to drive the optical modulators. Since at this stage the optical pulses are very short (less than a few hundred femtoseconds) and have not stretched through dispersive fiber, reasonable amounts of timing jitter (less than a few hundred picoseconds) in the electrical patterns driving the IM/PM pair should have little effect on the waveform generated.

According to the mathematical analysis provided in [19], in the far-field limit [19,27], the passband generated RF waveform, v(t), has the following profile:

$$v(t) \propto \sum_i A_i \times \left| H\left(\frac{-(t-iT)}{\psi_2} \right) \right| . \cos\left(\frac{(t-iT)\tau}{\psi_2} + \angle H\left(\frac{-(t-iT)}{\psi_2} \right) - \phi_i \right) \qquad (1)$$

where $H(\omega) = |H(\omega)| \angle H(\omega)$ is the pulse shaper spectral transfer function, T is the pulsed laser repetition period, τ is the variable delay, ψ_2 is the value of dispersion and the A_i's and ϕ_i's are individual elements of the amplitude/phase sequences encoded using the IM/PM pair. Additional baseband terms at the output of the PD are filtered using a high pass RF filter [19].

#235746 - $15.00 USD Received 5 Mar 2015; revised 20 Apr 2015; accepted 25 Apr 2015; published 30 Apr 2015

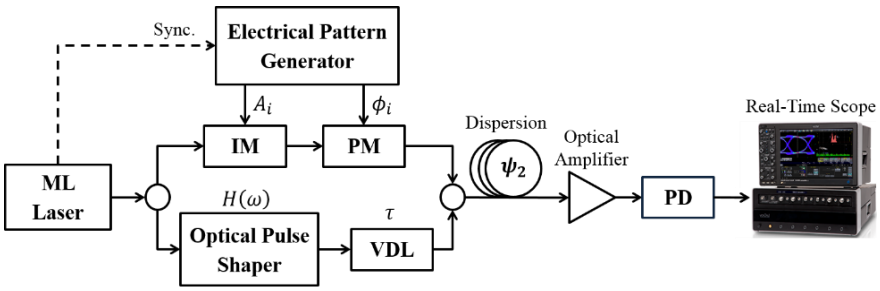

Fig. 1. Photonic-assisted RF-AWG schematic diagram.

As observed from (1), *v(t)* is a sequence of phase- and amplitude-modulated programmable RF waveforms with the same repetition rate as the pulsed laser. The center frequency of these waveforms (f_C) is set by tuning the value of τ according to $f_C = |\tau / 2\pi\psi_2|$, while their temporal amplitude and phase profile is set by the pulse shaper's spectral amplitude and phase. Furthermore, the driving voltages to the modulator pair control the relative phase and amplitude of each individual waveform within the generated sequence, independent from the RF-AWG stage. That is, the design of the arbitrary waveform, its center frequency, and an overall complex digital data modulation are controlled independently. This feature allows the simple implementation of various complex data modulation sequences, by adjusting the signal patterns driving the modulator pair. It is important to note that the effect of the modulators only appears in the amplitude and phase modulation parameters, A_i and ϕ_i, and does not modify the RF-AWG process.

In the following section we present experimental results demonstrating generation of ultrabroadband RF-arbitrary waveforms with frequency content up to ~52 GHz and spanning more than 4.7 octaves. We then overlay high-speed programmable data modulation, choosing as examples M-ary phase shift-keying (PSK) and quadrature amplitude modulation (QAM), in both cases with up to 16 levels (4 bits) per symbol. Although the center frequency and bandwidth of the generated RF waveforms can be easily scaled either to higher (with appropriate photodetection technology) or lower values, in this work we choose to show results that achieve the largest frequency content consistent with our available experimental equipment (photodetector and waveform digitizer). We have previously shown both mathematically [19] and experimentally [26] that the maximum achievable carrier frequency can be much higher (in principle more than several hundred gigahertz if an appropriate optical-to-electrical converter is available).

3. Experiments and results

In our experiments, we utilize a self-referenced mode-locked fiber laser (Menlo Systems FC1500-250-WG) with 250 MHz repetition rate and 15 dBm average power as the pulsed source. The pulses from this laser cover the full optical C-band (1525-1565 nm), which is also the operating range of our high-resolution optical pulse shaper (Finisar 1000SP) which features 1 GHz addressability and ~10 GHz resolution. The optical phase and intensity modulators each have a modulation bandwidth of ~10 GHz with a half-wave voltage of 2.9 V and 3.5 V at 1 GHz, respectively. The output pulses from the interferometric subsystem are stretched in ~6 km of single-mode fiber (SMF with total dispersion of ~100 ps/nm) and amplified (to ~10 dBm average power) in an erbium-doped fiber amplifier before beating on a high-speed photodetector (~52 GHz 3-dB bandwidth). The length of fiber is precisely chosen such that the generated RF arbitrary waveforms each span the available 4 ns time aperture, set by the repetition rate of the ML laser.

#235746 - $15.00 USD Received 5 Mar 2015; revised 20 Apr 2015; accepted 25 Apr 2015; published 30 Apr 2015

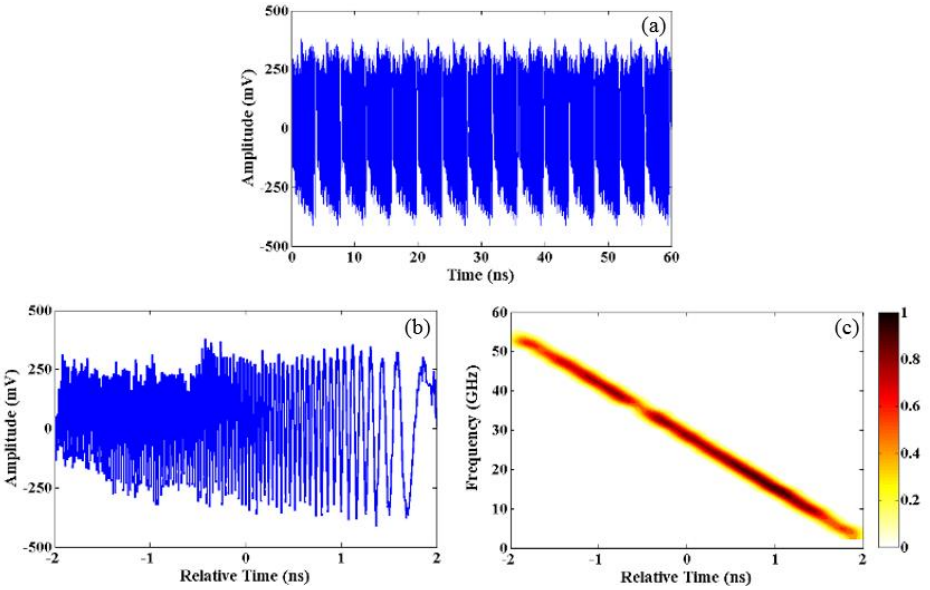

Fig. 2. Periodic repetition of ultrabroadband linear down-chirp waveform. (a) 60 ns-long real-time measurement of the generated sequence. (b) Temporal profile of an individual 4 ns-long, 50 GHz bandwidth RF chirp. (c) Normalized spectrogram plot of an individual RF chirp.

Finally, the RF waveform is filtered with a 50 kHz high pass filter and measured on a 65 GHz real-time oscilloscope with 50Ω input impedance.

3.1 Ultrabroadband radio-frequency arbitrary waveform generation

First, we provide experimental results for the case where no modulation is applied, i.e., $\phi_i = 0$ and $A_i = 1$ for all indices. Figure 2 illustrates a 60 ns-long measurement result for an ultrabroadband linear down-chirped RF waveform sequence, generated by applying a quadratic phase function in the pulse shaping stage, as well as compensating for the excess higher order dispersion of the SMF spool [19]. Each individual signal has a time duration of ~4 ns, while covering a 50 GHz 3-dB bandwidth from ~2 GHz to ~52 GHz, or equivalently ~4.7 octaves frequency span. Here, the average generated RF power is ~-0.45 dBm, which can be increased by amplifying more at the optical amplification stage and using a photodetector with higher optical power handling. The chirped pulses have a repetition rate of 250 MHz, equal to that of the ML laser. The spectrogram of a single 4ns-long waveform from Fig. 2(b) is calculated offline using a 200 ps Gaussian gate function and plotted in Fig. 2(c), showing close-to-perfect linearity of the RF waveform's instantaneous frequency versus time.

In the next subsections we demonstrate sequences in which the ultrabroadband linear down-chirp waveform of Fig. 2 is repeated, now adding programmable phase and amplitude modulation synchronized to the waveform repetition period.

3.2 Programmable phase modulation

To demonstrate programmable phase modulation, the A_i values are all set to 1 by biasing the IM at maximum transmission. Figure 3 shows the results of modulating a four-level drive signal to the PM in order to achieve 0°, 90°, 180° and 270° phase shift on the waveform of Fig. 2. To provide a clear illustration of the phase modulation effect, this figure includes zoom-in views to two 0.3 ns-long frames of the generated waveforms. It is worth mentioning that through the use of a high-speed PM, we can arbitrarily set the relative phase of individual waveforms within the generated RF sequence, independently, as expected from the derivation in (1).

#235746 - $15.00 USD Received 5 Mar 2015; revised 20 Apr 2015; accepted 25 Apr 2015; published 30 Apr 2015

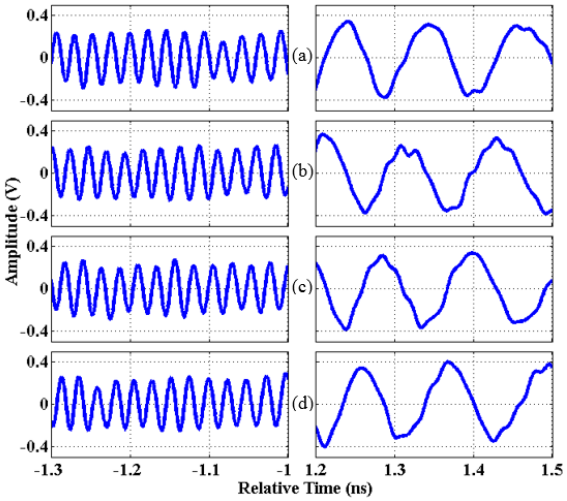

Fig. 3. Zoom-in views of the generated ultrabroadband RF waveforms with (a) 0°, (b) 90°, (c) 180°, and (d) 270° phase shift.

This phase modulation capability allows us to implement various phase-shift keying (PSK) schemes on the generated programmable RF waveforms. Figure 4 shows the measurement result for a binary-PSK (BPSK) data modulation experiment using this scheme. In this experiment, the ultrabroadband linear down-chirps of Fig. 2 are randomly modulated at 250 MHz by a binary sequence of length 1000. A color-coded 60 ns window of the resultant 4 μs-long measurement is plotted in Fig. 4(a), while Fig. 4(b) shows, within the same time range, the electrical data signal driving the optical phase modulator (normalized to the corresponding V_π). To clearly observe the 180° phase shifts between the generated antipodal BPSK signals, two individual anti-phase chirps are overlaid in the plot of Fig. 4(c), alongside zoom-in views.

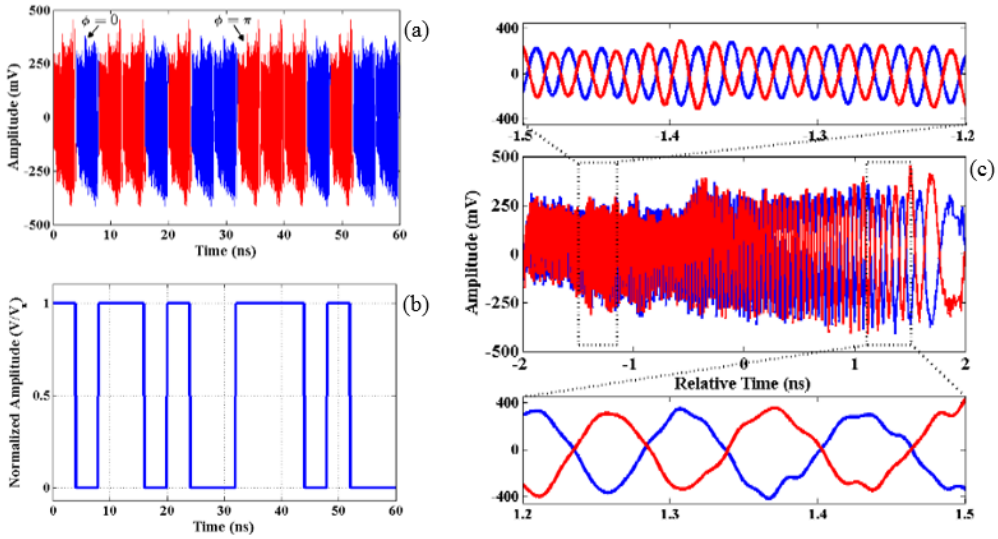

Fig. 4. Ultrabroadband BPSK measurement results – (a) Color-coded 60ns window of 4μs-long BPSK sequence. (b) Normalized bi-level electrical signal at the input of the phase modulator (V_π = 2.9V). (c) Overlay of generated antipodal chirps and zoom-ins.

#235746 - $15.00 USD Received 5 Mar 2015; revised 20 Apr 2015; accepted 25 Apr 2015; published 30 Apr 2015

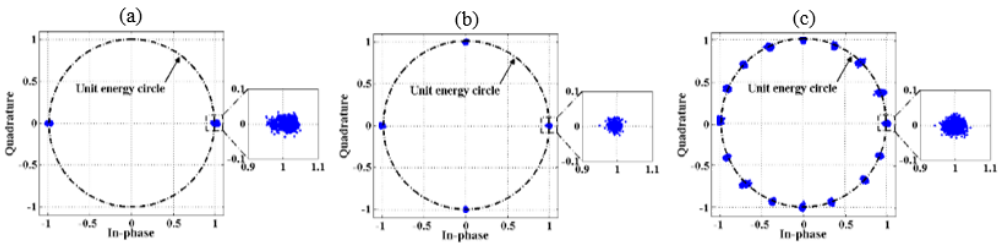

Fig. 5. Calculated signal constellations from long real-time measurements of various PSK scenarios and zoom-ins: (a) BPSK, (b) QPSK, (c) 16-PSK.

To demonstrate higher order modulation, we also carried out various experiments for quadrature-PSK (QPSK) and 16-level PSK on the same ultrabroadband signal. In all experiments, we use a length 1000 M-ary data sequence to drive the PM. For example, QPSK is accomplished by applying 4-level data sequences to switch between the waveforms of Fig. 3. It must be noted that from the application perspective, this preprogrammed sequence can be replaced by a real-time data sequence to be directly modulated, as different symbols, on the ultrabroadband signal. Also, such higher order modulation increases the communication data rate. Thus, our BPSK, QPSK and 16-PSK experiments have bit rates of 250 Mbps, 500 Mbps and 1 Gbps, respectively (1, 2, and 4 bit per symbol multiplied by the 250 MHz symbol rate).

To test the quality of ultrabroadband PSK modulation, we process the 4μs-long PSK sequence measurements to yield constellation plots, shown in Fig. 5. Each data point in these plots is the result of offline decoding of the amplitude and phase of each 4ns-long chirp in the PSK sequence. The amplitude of each waveform is derived by computing the square root of its total energy and normalizing it by the average computed amplitude over all waveforms in the sequence. To obtain the phase, we first assign zero phase to a reference waveform from the sequence. Then, for each chirp, we run an iterative procedure to decode the phase. In each step, we apply a constant phase shift to the chirp in the Fourier domain. Then, the phase-shifted signal is cross-correlated with the reference in the time domain and the peak value of cross-correlation is stored. This process is continued with a phase step of 0.5° from 0° to 360°. Finally, the inverse of the phase shift value that provides the maximum cross-correlation peak is assigned as the decoded phase of the each specific waveform. The constellation plot results indicate a high level of accuracy in phase shift keying modulation, with average error vector magnitudes (EVM [28]) over all the symbols calculated to be 2.36%, 2.01% and 3.22%, for BPSK, QPSK and 16-PSK, respectively. The slight errors are attributed to limitations in PM drive signal quality, noise induced in the optical amplification and photodetection stages, as well as a contribution from the real-time oscilloscope. Also, the small timing jitter between the two fiber-optic interferometer arms, may contribute slightly to the phase error. We have shown in [19] that by implementing a feedback stabilizer system and piezo-electric fiber stretcher, this small amount of jitter can be even further suppressed to negligible values.

3.3 Programmable phase and amplitude modulation

Going beyond the phase-only modulation demonstrated in the previous section, the setup of Fig. 1 is capable of simultaneous phase and amplitude modulation. As an example Fig. 6 exhibits results for an 8-level rectangular quadrature amplitude modulation (QAM) experiment (3 bits per symbol). Figure 6(a) shows the modulated waveform over a 60 ns time interval (15 individual chirp waveforms) in which all the symbols from the 8-QAM constellation appear at least once. The individual waveforms in the sequence are labeled to indicate their amplitude and phase. The corresponding drive signals to the IM and PM are normalized to the respective V_π values and plotted in Figs. 6(b) and 6(c). Note that the IM is initially biased at maximum transmission; and the IM drive signal of Fig. 6(b) corresponds to

#235746 - $15.00 USD Received 5 Mar 2015; revised 20 Apr 2015; accepted 25 Apr 2015; published 30 Apr 2015

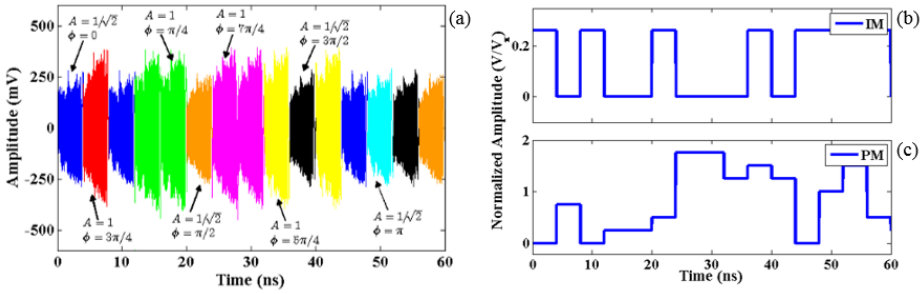

Fig. 6. Ultrabroadband 8-QAM measurement results – (a) Color-coded 60ns window of 4μs-long 8-QAM sequence. (b) Normalized electrical drive signal at the input of the IM (V_π = 3.5V), and (c) normalized electrical drive signal at the input of the PM (V_π = 2.9V).

the extra voltage applied to the modulator in order to reduce the transmitted power for certain symbols. In contrast to the phase modulation case, the IM drive signal requires equalization to compensate for the nonlinearity of conventional optical IMs. Alternatively, the IM/PM pair can be replaced with a linear I/Q modulator to obtain similar results without the requirement of an equalization stage [29].

Similar to the previous section, we take a 4 μs-long 8-QAM measurement and perform offline demodulation in order to plot the 8-point signal constellation in Fig. 7(a). Additionally, Figs. 7(b) and 7(c) show results for rectangular and circular 16-QAM experiments [30], both corresponding to four bits per symbol. The average EVM values over all symbols for Figs. 7(a)–7(c) are 2.56%, 3.01% and 3.21%, respectively. These error values show that the quality of the phase- and amplitude-modulated waveforms remains similar to the quality of phase-only modulation results presented earlier. Also, increasing the number of constellation points in the modulated sequence does not seem to affect the phase and amplitude modulation quality and may potentially be extended beyond the 16 symbols shown. Clearly, however, signal-to-noise considerations will eventually limit the number of useful modulation levels.

4. Conclusion

We have introduced a novel photonic-assisted radio-frequency arbitrary waveform generation setup, capable of overlaying high-speed phase and amplitude modulation on repetitions of the generated RF arbitrary waveform. The data modulation in our technique is independent from the RF-AWG signal design stage, allowing simple compatibility with real-time data sequences. First, the setup is utilized to generate an ultrabroadband linear frequency-chirped RF waveform with a bandwidth of 50 GHz, spanning more than 4.7 octaves. Then, through the use of high-speed optical phase and intensity modulators embedded in our generation setup, phase-shift keying (BPSK, QPSK and 16-PSK) and quadrature amplitude modulation (8-QAM and 16-QAM) tests are carried out to illustrate high-precision data modulation at 250 Mbaud symbol rate and up to 4 bits per symbol.

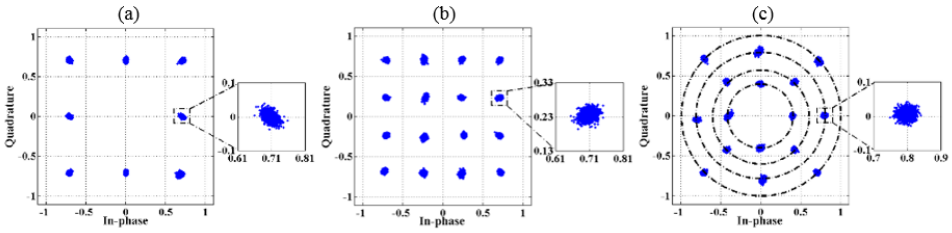

Fig. 7. Calculated signal constellation plots from long real-time measurements of various quadrature amplitude modulation scenarios and zoom-ins: (a) Rectangular 8-QAM, (b) Rectangular 16-QAM, and (c) Non-rectangular (circular) 16-QAM.

#235746 - $15.00 USD Received 5 Mar 2015; revised 20 Apr 2015; accepted 25 Apr 2015; published 30 Apr 2015

Note that since the RF waveform design is independent of the data modulation in our setup, the center frequency and/or bandwidth of the generated waveform sequence can be scaled to higher or lower values according to application needs. Furthermore, utilizing a higher repetition rate short pulse laser source would immediately allow a corresponding increase in the symbol rate.

Acknowledgments

The authors would like to thank Teledyne Lecroy Inc. for their loan of a 65 GHz, 160 GSa/s real-time oscilloscope (LabMaster 10-65Zi). This work was supported in part by the Office of the Assistant Secretary of Defense for Research and Engineering under the National Security Science and Engineering Faculty Fellowship program through grant N00244-09-1-0068 from the Naval Postgraduate School.

#235746 - $15.00 USD Received 5 Mar 2015; revised 20 Apr 2015; accepted 25 Apr 2015; published 30 Apr 2015